Studying the Solid-State Dynamics of Boron Compounds using Nuclear Magnetic Resonance (NMR) and MAS (Magic Angle Spinning).

Kyle E. Jeong

May 9, 2011

Abstract

The goal of this thesis is to study the solid-state molecular dynamics of 1,2-Dihydroazaborine-chromium tricarbonyl using ^{11}B Nuclear Magnetic Resonance (NMR) and Magic Angle Spinning (MAS) at 17.6 Tesla magnetic field strength. 1,2-Dihydroazaborine-chromium tricarbonyl is a derivative compound of 1,2-Dihydro-1,2-azaborine. It shares many of its mother compound's properties. However, unlike 1,2-Dihydro-1,2-azaborine, this derivative compound remains in its solid physical state at room temperature, which makes it possible to use MAS.

Borax compound is used to tune-up the experiment for the diazaborine trials, due to diazaborine's extreme sensitivity to atmospheric oxygen and water vapor. Using a solid-echo pulse sequence (90^o-τ-90^o), the ^{11}B NMR spectrum of borax was obtained, which shows the boron signal from its 3-coordinate and 4-coordinate boron sites, as well as the boron signal originating from the BN crucible in NMR probe. Using zero-go-background-suppression with a solid-echo sequence and the composite 90^o, the background boron signal was almost completely suppressed, though it did tend to suppress much of the side transition peaks as well. The NMR line shape was simulated

for ^{11}B central transition ($-\frac{1}{2} \leftrightarrow \frac{1}{2}$), using the published values of quadrupolar coupling constant and the asymmetry of the electric field gradient tensor.

The ^{11}B NMR spectrum of diazaborine showed an order of magnitude greater line width than that of the simulated diazaborine spectrum, and its center peak looked similar to borax's 3-coordinate boron site peak. A long T_1 relaxation time was also estimated, which indicates the absence of the fast-paced planar jumping motion of the diazaborine, which was expected at room temperature. These two observations indicate that the diazaborine sample might have degraded during preparation and/or the long experiments.

Acknowledgement

I am most grateful to Drs. Vold and Hoatson for this opportunity, which allowed me to conduct my thesis project in the NMR laboratory of the College of William and Mary. I particularly appreciate the enormous amount of time, that Dr. Vold spent to help me set up and perform the NMR experiment, as well as his generous and patient tuition. I am also thankful to the lab members, especially Jeremy Weeden and Christopher Maher for their help. Finally, I am grateful for the strong support from my parents.

Chapter 1. INTRODUCTION

When a new chemical material is synthesized, it is crucial to understand its physical properties, which include structure, electrical and mechanical properties, and dynamics of the molecules, in order to further improvement development of the material. Although structural information can be obtained using various techniques, such as X-ray and electron microscopy, there are not as many methods to study dynamics. Nuclear magnetic resonance (NMR) is one of few tools to study molecular dynamics over a very wide time scale. NMR parameters, such as the spin-lattice relaxation time T_1, spin-spin relaxation time T_2, and the interactions that determine the NMR line shape, are generally motion-dependent. The molecular motion can be varied by varying the physical environment of the sample, such as the temperature and the pressure.

T_1 describes the efficiency of the interaction between the spin system and its surrounding molecular environment, via interactions such as nuclear dipole-dipole coupling, and coupling of nuclear electric quadruple moments to local electric field gradients. These interactions change with varying molecular motion. Depending on the material, one interaction may dominate all others. In particular, one can study the activation energy of a specific type of motion by analyzing NMR parameters, such as T_1 or line width vs temperature. Hence, by analysis of the E_A, the molecular movement of different materials can be studied. The material under investigation in this case was 1,2-Dihydro-1,2-azaborine. By obtaining the spectral width Δf at different sample temperatures T, we can plot $1/\Delta f$ vs. T to acquire the slope, which represents the activation energy.

The aim of the research described in this thesis was to quantitatively examine the dynamics of a chemical compounds containing the element boron. Samples of 1,2-Dihydro-1,2-azaborine: C_4BNH_6 (diazaborine for short) and related materials were generously provided to us by Prof. Shih-Yuan Liu (Department of Chemistry, University of Oregon). Diazaborine is a hybrid compound of benzene (C_6H_6) and borazine $B_3N_3H_6$ (1,2). Each diazaborine molecule contains one boron nucleus, which is covalently bonded to a carbon, hydrogen, and nitrogen.

Boron-11 (^{11}B) has 80.42 % natural abundance and the nuclear spin quantum number I = 3/2 that possesses not only a magnetic dipole moment, but also an electric quadrupole moment. The nuclear dipole interacts with the external magnetic field by the Zeeman interaction and also other adjacent nuclear dipole moments via the dipole-dipole interaction. In addition, the electric quadrupole moment interacts with electric field gradients that may be present at the site of the nuclei. The static terms of both dipole-dipole and quadrupole interactions depend on $(3\cos^2\theta - 1)$, where θ is the angle between the external magnetic field $\mathbf{B}_o$ and the radial vector connecting two dipoles for the dipole-dipole interaction or z-axis of the principal axis system of the electric field gradient tensor. Magic angle spinning (MAS) can effectively remove these static terms by rapidly spinning the sample during the NMR measurement (3).

Because it has a planar structure very similar to benzene with altered bond lengths, in-plane jumping with six-fold symmetry is expected. The expected NMR spectra were simulated using the simulation software, Express (4), for 2-site and 6-site jumping motions, using the previously measured values of asymmetry η and quadrupole coupling constant C_Q by Daly, et al (1).

The NMR probe contains a boron nitride crucible, which sits inside the RF coil to hold the samples. It is therefore important to conduct NMR experiments to characterize the ^{11}B NMR of the background, that is, without the sample. In addition, a series of NMR experiments was performed with Borax, $Na_2B_4O_7.10H_2O$ as a tune-up sample, before embarking on the more difficult study of the air and moisture sensitive diazaborine materials.

Chapter 2. Diazaborine (1,2-dihydro-1,2-azaborine: C_4BNH_6)

Diazaborine (1,2-Dihydro-1,2-azaborine: C_4BNH_6) is a hybrid compound of benzene (C_6H_6) and borazine $B_3N_3H_6$ (1,2). One C-C bond of benzene is replaced by a B-N bond. The material has a planar structure similar to benzene, with altered bond lengths. As listed in table 1, bond lengths between various adjacent pairs of nuclei are modified from 1.40 Á of the C-C bond in benzene, to 1.45 Á for B-N, 1.51 Á for B-C, and 1.37 Á for N-C bond, respectively. This indicates that the B-N bond is less strong than a C-C bond. The inner angles between two adjacent bonds change from 120^o of the benzene ring to 119^o (C-C and B-C), 114 ~ 115^o (C-B and B-N), 123^o (B-N and N-C), and 120^o (N-C and C-C) (1).

Diazaborine-based compounds may have very different physical properties from benzene-ring based organic compounds. For example, the melting temperature of pure diazaborine is -46 ~ -45 ^oC, which is considerably lower than that of benzene (5^o C).

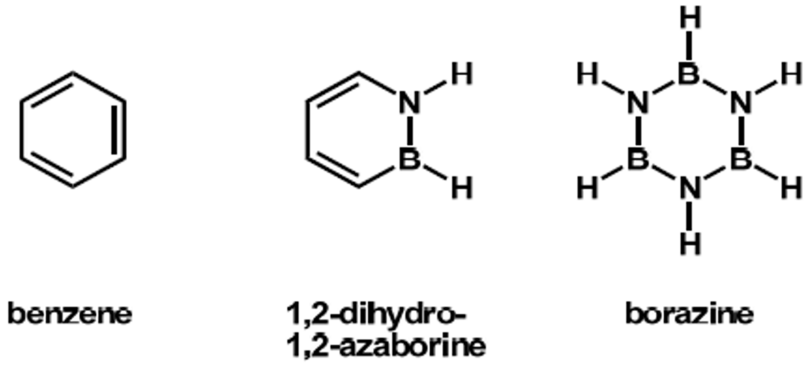

Figure 1. *Chemical structures of benzene, diazaborine (1,2-dihydro-1,2-azaborine, and borazine. One, or all, of the C-C bonds are replaced by B-N bonds in diazaborine and borazine, respectively.*

It is worth noting that diazaborine is known to be extremely sensitive to moisture and air, and will degrade when exposed to the atmosphere. 1,2-Dihydroazaborine-chromium tricarbonyl is a derivative compound of 1,2-Dihydro-1,2-azaborine. It has a similar chemical structure to benzene chromium tricarbonyl, with the hexagonal planar ring structure bonded with chromium tricarbonyl, $Cr(CO)_3$, as shown in Fig. 2. Conveniently, this derivative compound does not have the melting temperature of -45 °C but remains in its solid physical state at room temperature. This allows one to apply MAS to the compound at room temperature. The quadrupolar constant C_Q and the asymmetry constant η of this compound were determined as 1.25 MHz and 0.256, respectively, by Daly (1). Daly, et. al., worked with diazaborine directly (in the gas phase). It is a good assumption that the C_Q and η for the chromium complex are not very different from the values they measured. With these two constants, one should be able to compare the acquired experimental spectrum and the simulated spectrum to confirm the legitimacy of the obtained experimental spectrum.

Table 1. *Summary of benzene, diazaborine (1,2-Dihydro-1,2-azaborine), and borazine.*

	benzene	*diazaborine*	*borazine*
chemical formula	C_6H_6	C_4BNH_6	$B_3N_3H_6$
bond length (Á)	C-C: 1.40	B-N: 1.45 B-C: 1.51 N-C: 1.37	B-N: 1.44
melting point (^oC)	5	-45	-58

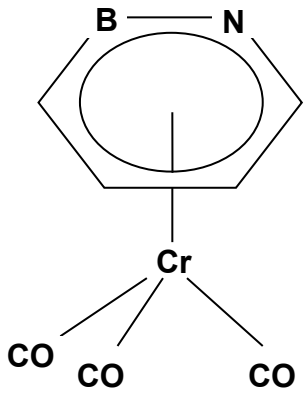

Figure 2. *Chemical structures of 1,2-Dihydroazaborine-chromium tricarbonyl, a derivative compound of 1,2-dihydro-1,2-azaborine..*

Chapter 3. BASIC THEORY OF NMR

The nuclear spin states are degenerate in a zero external magnetic field, which indicates that multiple spin states occupy the same energy level. The degeneracy is lifted once a non-zero $\vec{B}$ is applied to the spin states, a process known as the Zeeman effect.

3.1. Nuclear Zeeman Interaction (3,5)

A nucleus with non-zero nuclear spin quantum number I possesses the nuclear magnetic moment given by $\vec{\mu} = \gamma\hbar\,\vec{I}$. Here, γ is the gyromagnetic ratio that is different for different nuclei. This magnetic moment $\vec{\mu}$ interacts with the external magnetic field $\vec{B}_o = B_o\,\hat{z}$, as described by the Zeeman interaction,

$$U = -\vec{\mu}\cdot\vec{B}_o = -\gamma\hbar B_o I_z. \qquad \ldots\ldots [1]$$

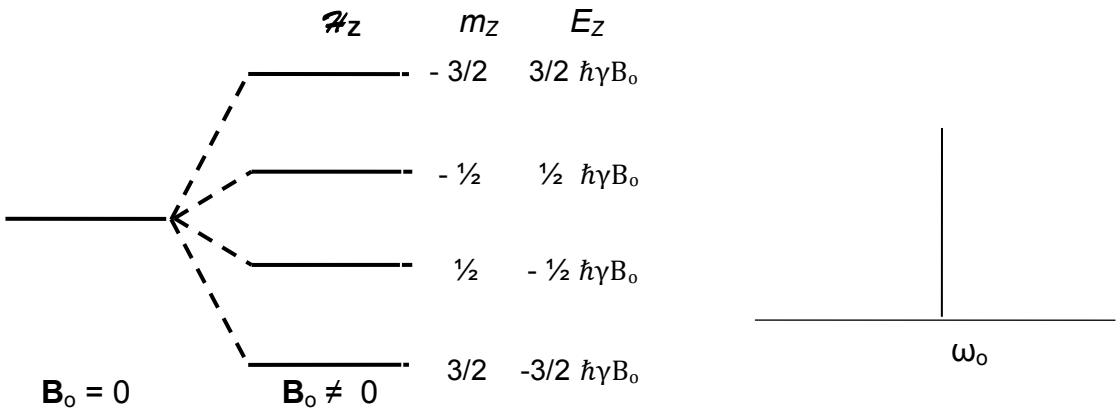

Figure 3. *Energy diagram of Zeeman interaction for a spin I = 3/2. The four degenerate spin states, i.e., m_z = -3/2, -1/2, 1/2 and 3/2, are shifted by a non-zero external magnetic field $B_o \neq 0$ to energy levels, $U = -\vec{\mu}\cdot\vec{B}_o = -\hbar\gamma B_o m_z$. The difference between two adjacent energy levels is $\Delta E = \hbar\gamma B_o = \hbar\omega_o$.*

Eq. [1] indicates that the energy level of the Zeeman interaction depends on the z component m_z of the spin angular momentum. For instance, ^{11}B possesses nuclear spin I = 3/2 and the Zeeman energy levels are split into four states, $U_z = -\gamma\hbar B_o m_z$, with $m_z = \frac{3}{2}, \frac{1}{2}, -\frac{2}{1}, -\frac{3}{2}$. These energy levels are illustrated in Fig. 3.

When bulk matter is placed within an external magnetic field, a net magnetization $\vec{M}$ is built along the field $\vec{B}_o$ as (6),

$$\vec{M} = \frac{N\gamma^2\hbar^2 I(I+1)}{3kT}\vec{B}_o \text{ (Curie's law of magnetization),} \quad \ldots\ldots \quad [2]$$

which indicates that the available magnetization increases linearly with magnetic field and is inversely proportional to the temperature. NMR measures the signal that is a function of the magnitude of the thermal magnetization, the NMR properties such as T_1 and T_2, and NMR (Larmor) frequency. Radio-Frequency (RF) energy is applied to flip the net magnetization, which is aligned along the longitudinal direction, toward the transverse plane. The NMR signal is then measured on the transverse magnetization.

3.2. Bloch's Equation (3,5,6)

At thermal equilibrium, the magnetization that is built along the static magnetic field $\mathbf{B}_o$, is $\boldsymbol{M_o} = (0, 0, \frac{C}{T}\boldsymbol{B_o})$, where C is Curie's constant $C = \frac{N\gamma^2 I(I+1)}{3k}$, N the total number of nuclei, k the Boltzman constant, and T temperature. When its equilibrium state is disturbed, the magnetization vector experiences a torque, which is exerted by the external

magnetic field $\mathbf{B}_o = B_o\mathbf{z}$, and the relaxation processes toward its thermal equilibrium. Bloch's equation describes these processes as,

$$\frac{d\boldsymbol{M}}{dt} = \gamma \boldsymbol{M} \times \boldsymbol{B}_o + \frac{M_o - M_z}{T_1}\,\hat{z} + \frac{M_x\hat{x} + M_y\hat{y}}{T_2} \qquad \ldots\ldots \text{[3]}$$

The magnetization vector **M** precesses about the external magnetic field with the Larmor frequency $\omega_o = \gamma B_o$. Thus Bloch's equation can be split to longitudinal (z) and transverse (x, y) components as,

$$\frac{dM_z}{dt} = \gamma\left(\vec{M} \times \vec{B}_o\right)_z + \frac{M_o - M_z}{T_1}, \qquad \ldots\ldots \text{[4a]}$$

$$\frac{dM_x}{dt} = \gamma\left(\vec{M} \times \vec{B}_o\right)_x + \frac{M_x}{T_2}, \qquad \ldots\ldots \text{[4b]}$$

$$\frac{dM_y}{dt} = \gamma\left(\vec{M} \times \vec{B}_o\right)_y + \frac{M_y}{T_2} \qquad \ldots\ldots \text{[4c]}$$

Here, T_1 and T_2 are longitudinal and transverse relaxation times, respectively. Eq. [4a] indicates a recovery process with the characteristic time T_1 that is related to the transfer of energy from the spin-system to the lattice that is the rest of the energy reservoir. T_1 can also be described as the characteristic time for the interrupted spin system to recover to its longitudinal thermal equilibrium magnetization M_o. Eqs. [4b] and [4c] indicate a decay process toward its equilibrium transverse magnetization of zero with the characteristic time T_2.

These relaxation times, particularly T_1, are sensitive to molecular motion. Hence, by examining the T_1 relaxation time of ^{11}B in a boron compound versus temperature, the

dynamics of a molecule can be studied. In addition, the shape of the Fourier transformation of the time-domain NMR signal provides the absorption spectrum. Changes in the physical environment, such as temperature, also lead to changes in the width and the shape of the spectrum.

3.3. Perturbation (7)

NMR of the nucleus with a spin quantum number greater than ½ is influenced by various local interactions, such as the nuclear quadrupole interaction, which is the interaction between the electric quadrupole moment of the nucleus and the crystal electric-field gradient, and dipole-dipole interactions from nearby nuclear dipoles. For instance, the boron nucleus in diazaborine experiences dipole-dipole interactions from its adjacent hydrogen, nitrogen, and carbon.

Here, the nuclear quadrupolar and the dipole-dipole interactions act as perturbations to the main Zeeman interaction as, $\mathbf{H = H_Z + H_Q + H_D}$.

Table 2. *Electric and magnetic multipole moments of spin quantum number I.*

Spin (I)	*Monopole*	*Dipole*	*Quadrupole*	*Octapole*
0	Electric	0	0	0
$^1/_2$	Electric	Magnetic	0	0
1	Electric	Magnetic	Electric	0
$^3/_2$	Electric	Magnetic	Electric	Magnetic

3.3.1. Nuclear Quadrupolar Interaction: Nuclei with spin-quantum numbers greater than ½ possess both magnetic dipole and electric quadrupole moments, as listed in Table 2. The anisotropic interaction occurs in solids between the electric quadrupole moment and the electric field gradient (EFG), which originates from the electronic charge distribution in the system. The quadrupolar Hamiltonian $\mathbf{H_Q}$ is given by (3),

$$H_Q = \frac{eQ}{2I(2I-1)\hbar}\vec{I}\cdot\breve{V}\cdot\vec{I} \qquad \ldots\ldots \quad [5]$$

$\vec{I}\cdot\breve{V}\cdot\vec{I}$ in eq. [5] represents the scalar product from the nuclear spin vector and the second-order EFG tensor. The EFG tensor, $\breve{V}$, can be written as,

$$\breve{V} = \begin{pmatrix} V_{xx} & V_{xy} & V_{xz} \\ V_{yx} & V_{yy} & V_{yz} \\ V_{zx} & V_{zy} & V_{zz} \end{pmatrix} \qquad \ldots\ldots \quad [6]$$

It is important to note that this quadrupolar interaction can be described in simple form in the principal axis system (PAS) of the EFG tensor. In PAS, the electric field gradient tensor $\breve{V}$ is diagonalized with the diagonal elements V_{xx}, V_{yy} and V_{zz} as the only non-zero tensor components. In this principal axis system, the static term of the quadrupolar Hamiltonian is simplified as,

$$H_Q^{PAS} = \frac{3eQV_{ZZ}}{4I(2I-1)\hbar}\left[I_Z^2 - \frac{I^2+I}{3} + \frac{\eta}{3}(I_X^2 - I_Y^2)\right] \qquad \ldots\ldots \quad [7]$$

Here, η represents the asymmetry, $\eta = (V_{xx} - V_{yy})/V_{zz}$ with $0 < \eta < 1$. X, Y, and Z are the principal axes of the EFG tensor.

It is convenient to transform the PAS reference frame to the frame of reference in which the z-axis is parallel to the external magnetic field $\mathbf{B}_o$ (6). Then, the eq. [7] becomes,

$$H_Q = \frac{9C_Q}{8I(2I-1)}(3cos^2\theta - 1)\left(I_z^2 - \frac{1}{3}I(I+1)\right) \quad \ldots\ldots \quad [8]$$

Here, θ is the angle between the unique principal axis of the electric field gradient tensor and the external magnetic field $\mathbf{B}_o$. C_Q, the magnitude of the quadrupolar coupling, is approximately 0 to 30 MHz (8) and can be expressed as the following,

$$C_Q = \frac{eQV_{ZZ}}{h} = \frac{eQeq}{h} \quad \ldots\ldots \quad [9]$$

This $\mathbf{H_Q}$ gives the shift in the Zeeman energy levels in first order perturbation theory. The shifted energy level is illustrated in Fig. 4 for I = 3/2.

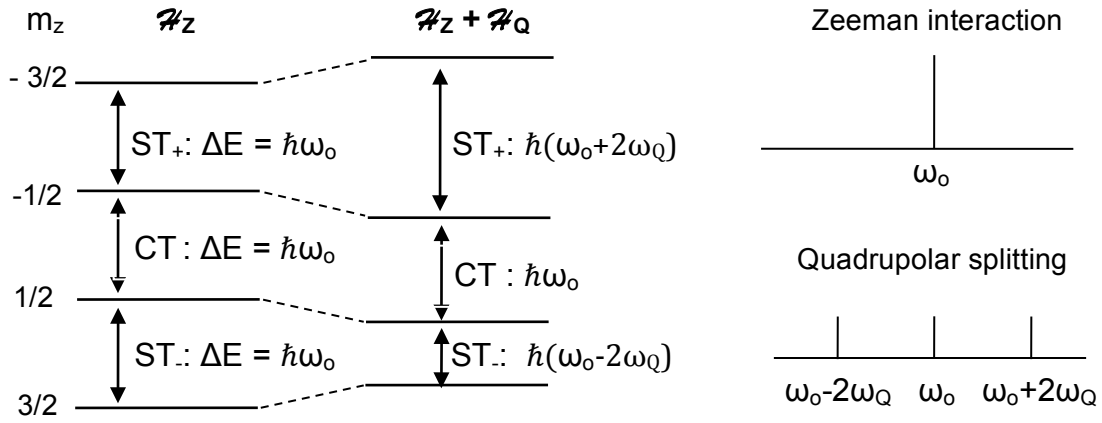

Figure 4. *Transition energies of central (CT) and two satellite (ST_- and ST_+) transitions of spin I = 3/2 system with and without the first-order quadrupolar interactions. All three-transition energies in the Zeeman interaction are identical. The first-order quadrupolar interaction symmetrically shifts the transitions 3/2 ↔1/2 and -3/2 ↔ -1/2 by equal amounts of energies, $2\hbar\omega_Q$. The expected spectra for the Zeeman interaction without and with the quadrupolar perturbation are shown.*

Although the quadrupolar contribution to the Hamiltonian can be large, it is usually significantly smaller than the Zeeman Hamiltonian in high magnetic fields, such as B_o = 17.6 T. Therefore, its effect on the energy levels can be described as a perturbation to the Zeeman energy levels. The mathematical expression, $E = E_Z + E_Q$, represents the first-order approximation of the energy level. Because the samples that are studied and examined in this project are ^{11}B compounds, the paper will focus on the case of I = 3/2, as shown in Fig. 4.

3.3.2. Second-Order Perturbation in Quadrupolar Interaction (3,8)**:** When the perturbed interaction is large or the sample is spun about the magic angle (54.7^{o}) during NMR data acquisition, the first-order quadrupolar correction to the Hamiltonian described above will not be sufficient to accurately describe the system. At this point, the next higher-order correction term may need to be considered as,

$$E = E_Z + E_Z^{(1)} + E_Z^{(2)} \qquad \ldots\ldots \quad [10]$$

The second-order quadrupolar correction is significantly smaller than the first-order contribution to the Hamiltonian, except for the central transition ($-½ \leftrightarrow ½$), for which the first order correction vanishes identically in MAS experiments.

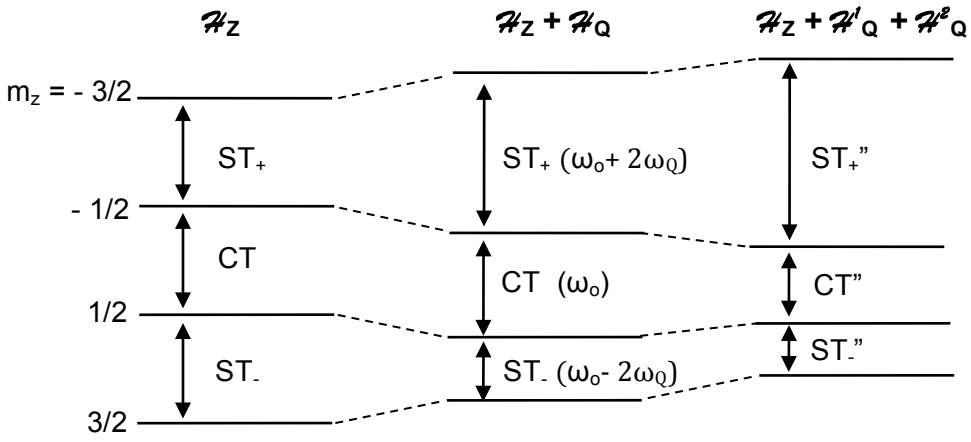

Figure 5. *The second-order quadrupolar interaction further shifts the energy levels of the Zeeman and the first-order quadrupolar interactions. Unlike the first-order quadrupolar shift, the second-order quadrupolar shifts are not symmetric about the Zeeman splitting. Even the central transition (CT") is broadened.*

The second–order quadrupolar frequency for an energy level can be described by the following equation below, where η_Q is assumed to be zero (8). *(Copied from lecture note "Introduction to Quadruploar NMR" by Sharon Ashbrook, Department of Chemistry, University of St Andrews)*

$$\omega \propto \frac{\left(\omega_Q^{PAS}\right)^2}{\omega_0} \cdot [A + B \cdot d_{00}^2(\beta) + C \cdot d_{00}^4(\beta)] \qquad \ldots\ldots \ [11]$$

$\frac{\left(\omega_Q^{PAS}\right)^2}{\omega_0}$ is a constant that is dependent on C_Q, I and ω_0. *A* denotes the isotropic shift, $B \cdot d_{00}^2(\beta)$ represents a second-rank anisotropic term that is proportional to ($3\cos^2\theta$ - 1), and $C \cdot d_{00}^4(\beta)$ represents a fourth-rank anisotropic term that is proportional to ($35\cos^4\theta - 30\cos^2\theta + 3$). The three factors, *A, B* and *C* listed in Table 2 are known constants and different for different nuclear spin quantum numbers. Also, the line shape of the central-transition, i.e., ½↔ - ½ of I= 3/2 for different non-zero η values can be referenced for further investigation of the experiment's results.

Table 3. *Coefficients for the second-order quadrupolar interactions for central- and sideband-transitions. (Copied from lecture note "Introduction to Quadruploar NMR" by Sharon Ashbrook, Department of Chemistry, University of St Andrews)*

Spin (I)	*transition*	*A*	*B*	*C*
3/2	CT	-2/5	-8/7	54/35
	ST	4/5	4/7	-48/35

3.3.3. Nuclear Dipole-Dipole Interaction: The two nuclear magnetic moments, $\vec{\mu}_1$ and $\vec{\mu}_2$, interact with each other over space. The strength of the dipolar coupling depends on the distance between two dipole moments by $1/r^3$, where r represents the distance between the two dipoles. Dipolar coupling is very helpful for studying molecular structures and dynamics, as we can learn about the internuclear distances. In liquid or gaseous states of a matter, this dipole-dipole interaction is averaged to zero by rapid isotropic molecular tumbling. However, in solids in which the characteristic hopping time of the molecular rotational or translational motion is slow, this is not the case. In solids there is significantly less molecular tumbling compared to liquid and gaseous states, causing line broadening.

The magnitude of the dipole Hamiltonian, $\mathbf{H_D}$, is usually significantly smaller than that of the Zeeman Hamiltonian. For instance, the size of typical dipole-dipole interactions in a solid is measured in the order of tens of kHz in frequency, while the Zeeman transition energy of ^{11}B nucleus in B_o = 17.6 Tesla is 245 MHz. Thus, it can be considered as a perturbation to the Zeeman interaction. The equation below illustrates the interaction energy, U_d, between the magnetic dipole moments, $\vec{\mu}_1 = \gamma_1 \hbar \overrightarrow{I_1}$ and $\vec{\mu}_2 = \gamma_2 \hbar \overrightarrow{I_2}$ (9),

$$U_d = \frac{\vec{\mu}_1 \cdot \vec{\mu}_2 - 3(\vec{\mu}_1 \cdot \hat{r}) \cdot (\vec{\mu}_2 \cdot \hat{r})}{r^3} \qquad \ldots\ldots \quad [12]$$

where $\vec{r}$ is the radial vector between the two magnetic dipole moments. Eq. [12] can be expressed as an operator as follows,

$$H_d = \frac{\gamma_1 \gamma_2 \hbar^2}{r^3} \cdot (A + B + C + D + E + F) \quad \ldots\ldots [13]$$

where the A, B, C, D, E, and F terms are as listed below (6),

$$A = -I_{1z} I_{2z} (3cos^2\theta - 1),$$

$$B = \frac{1}{4}(I_1^+ I_2^- + I_1^- I_2^+)(3cos^2\theta - 1),$$

$$C = -\frac{3}{2}(I_1^+ I_{2z} + I_{1z} I_2^+) sin\theta cos\theta e^{-i\varnothing},$$

$$D = -\frac{3}{2}(I_1^- I_{2z} + I_{1z} I_2^-) sin\theta cos\theta e^{i\varnothing}, \quad \ldots\ldots [14]$$

$$E = -\frac{3}{4} I_1^+ I_2^+ sin^2\theta e^{-2i\varnothing},$$

$$F = -\frac{3}{4} I_1^- I_2^- sin^2\theta e^{2i\varnothing}.$$

Here, θ represents the angle between the external magnetic field and the radial vector that connects two dipole vectors $\vec{\mu}_1$and $\vec{\mu}_2$. A and B terms are diagonal for like spins, and the A term is diagonal with respect to the Zeeman Hamiltonian's eigenstates. The other four terms, C, D, E, and F are off-diagonal so they may be important for spin-lattice relaxation but not for the transition frequencies and the line shape.

It is important to recognize that for our studies, the ^{11}B spectrum of the diazaborine will have three contributors to the dipolar coupling, ^{11}B's interaction with three adjacent elements: N, C, H. Due to the fact that only ^{13}C has a magnetic dipole moment and this isotope is only 1.109% naturally abundant, its contribution to the boron spectrum is negligible. For the other two cases, ^{1}H has a much greater gyromagnetic ratio, $267.513 \cdot 10^6$ rad $s^{-1} \cdot T^{-1}$ than ^{14}N, which has a gyromagnetic ratio of $19.331 \cdot 10^6$ rad $\cdot s^{-1} \cdot T^{-1}$.

Thus, the interaction from the hydrogen nucleus is the dominant dipole-dipole interaction on the ^{11}B nucleus, assuming that the separations between each nucleus and the boron are similar.

3.3.4. Powder Angle (3)**:** The relative orientation of a crystalline PAS with respect to the static magnetic field is represented as (θ, ϕ) in the lab frame as shown in Fig. 6a, and determines the strength of the quadrupolar interaction. In a powder sample, this orientation is uniformly distributed over a spherical surface. With the specific angle θ, the static term of the H_Q is proportional to $(3\cos^2\theta - 1)$ as described in eq. [8], with the population density *sinθ*, as shown in the Fig. 6b.

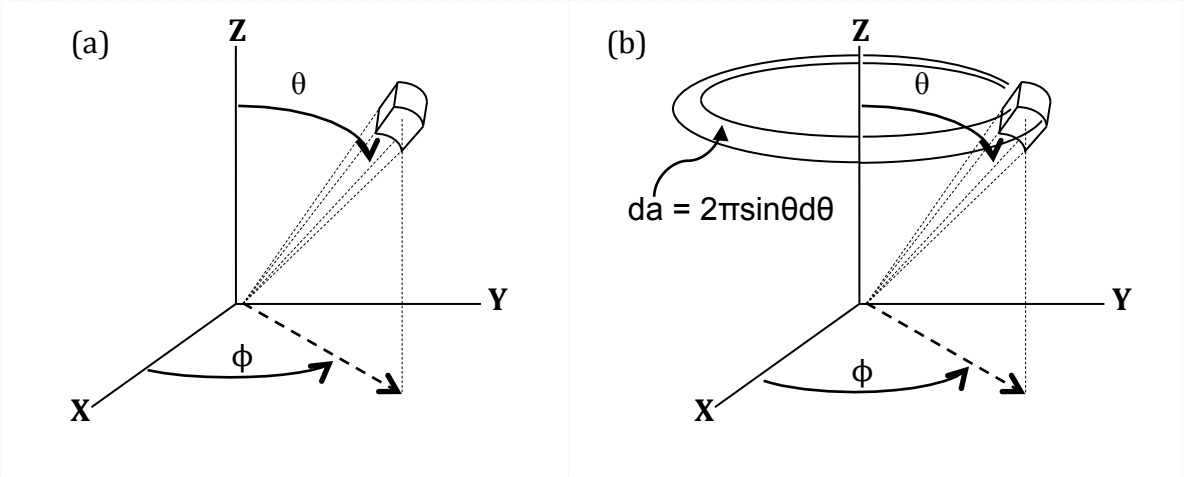

Figure 6. *Orientation of the quadrupolar interaction, and the density (or surface area) of the thin strip that is oriented along the azimuthal angle θ.*

3.3.5. Magic Angle Spinning (MAS): The static (or secular) terms of both quadrupolar and dipole-dipole interactions have the identical angular dependency $(3\cos^2\theta - 1)$ as in

eq. [8] and the terms *A, B* of eq. [14]. The broadening by these contributions may be removed by making $(3\cos^2\theta - 1) = 0$ by rapid spinning of the sample along $\theta = 54.7^o$, which is called the magic angle. The required spinning rate is determined by the line width of the solid NMR spectrum.

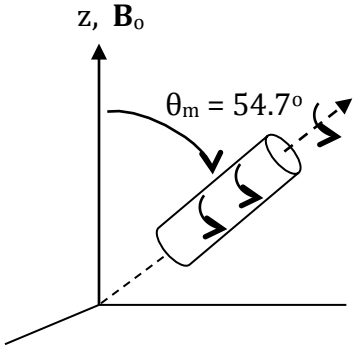

Figure 7. *Magic Angle Spinning (MAS): The sample is rapidly spun about the angle 54.7^o from the external magnetic field with a spinning rate of a few tens kHz.*

Chapter 4. MATERIALS AND METHODS

4.1. Materials

Borax ($Na_2B_2O_7{\cdot}4H_2O$) and Diazaborine (1,2-Dihydro-1,2-azaborine: C_4BNH_6) were used in this project. Borax was mainly used to tune up the spectrometer, i.e. to determine suitable data acquisition parameters and to investigate the interfering background signal.

Because 1,2-Dihydroazaborine-chromium tricarbonyl is a solid at room temperature, the sample is amenable to MAS experimentation. The sample was always stored within a vessel filled with nitrogen gas to prevent exposure of the sample to the air and moisture; otherwise the sample may degrade to a boron-oxygen compound. Unfortunately, these precautions proved to be insufficient, as will be described later.

4.2. Simulation of Power Pattern

The MAS powder line shape of ^{11}B NMR of the diazaborine was simulated using Express (4), which was developed by Drs. Vold and Hoatson at the College of William and Mary using MatLab (Mathworks, Natick, MA). The simulation was performed for a planar motion with a 60^o rotational jump about the axial axis with various quadrupolar coupling constants C_Q = 0.5, 1.0, 2.0, and 3.0 MHz, 10 kHz MAS spinning-rate, and a fixed asymmetry η = 0.256 of the electric-field gradient (determined by Daly et. al.,) (1).

4.3. NMR Experiments

All experiments were conducted at 240.685 MHz, the Larmor frequency of ^{11}B in a 17.6 Tesla magnet (Bruker BioSpin GmbH, Ettlingen, Germany), which is housed in the

NMR lab of the College of William and Mary. A probe capable of spinning 2.5 mm samples at up to 35 kHz was used. A 90^o- τ – 90^o solid-echo pulse sequence shown in Fig. 8 was used with pulse duration of 1.36 μs and τ = 40 μs (separation between two 90^o pulses). The other NMR experimental parameters included spectral bandwidth of 2.0 MHz, number of data samples of 8192 or 16384, and MAS spinning rate 10 kHz. The sample was maintained at a constant temperature of 300 K by a flow of dry nitrogen gas.

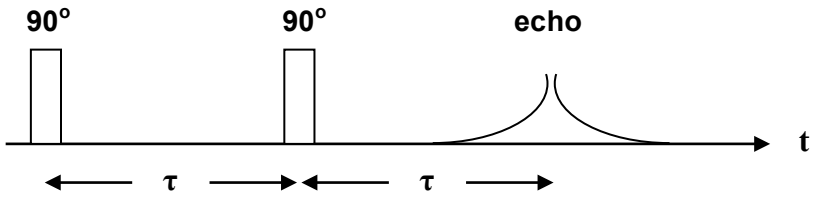

Figure 8. *ZG (zero-go) utilizes 90^o - τ – 90^o solid-echo pulse sequence. The duration of each RF pulse was 1.36 μs. This sequence is repeated for number of signal averaging (NS) every recycling time.*

The acquisition method ZGBS (zero-go-background-suppression) measures the NMR signal while suppressing the background signals originating outside the receiver coil. The method uses a composite 90^o pulse, consisting of a 90° and two 180° pulses with appropriate phase cycling (10). The phase cycled composite pulse is effectively a 90° pulse for all spins inside the coil and 0° for all spins outside of the coil. Thus, ideally, the measured signal is expected to represent the magnetization from the sample.

The rotor or the capsule containing the sample was inserted into the NMR probe. An appropriate filter was selected for the ^{11}B spectrum.

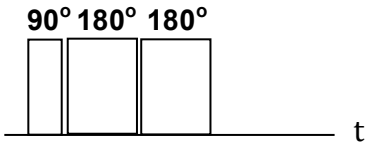

Figure 9. *Composite 90^o RF pulse is used for background suppression.*

A PSW ($Pb(Sc2/3W1/3)O_3$) sample was used to investigate the background ^{11}B signal. PSW does not contain ^{11}B, which in turn makes this series of tests no different from the case of an empty probe. Yet, unlike with an empty probe, with the PSW rotor, we can actually utilize the MAS to see the effects of the magic angle spinning on the spectral width. With PSW experiments, the goal was to measure the ^{11}B NMR spectrum of the sample in a 2.5 mm rotor with and without the background suppression pulse sequence in order to inspect the source of the background boron signal that appeared on the experimental results. The first experiment with PSW utilized the ZG pulse sequence with and without using MAS. The measurement was repeated without MAS, but with background suppression.

Borax ($Na_2B_2O_7{\cdot}4H_2O$) was used to tune the spectrometer, in preparation for experiments on the 1,2-Dihydroazaborine-chromium tricarbonyl sample. As a tune-up sample it is a great selection because of its high signal/noise ratio, low air and water sensitivity, high melting point, as well as low toxicity. Fig. 10 illustrates the chemical structure of $Na_2B_2O_7{\cdot}4H_2O$. A borax molecule has two specific boron sites as shown in its chemical structure: 3-coordinate and 4-coordinate. ^{11}B NMR was conducted on a borax sample in a 2.5 mm rotor with MAS - 30 kHz spinning rate, number of signal

averagings 64, recycling time of 4 seconds and 2.5 μs of 90° RF pulse width at 330 K. Background suppression was not applied.

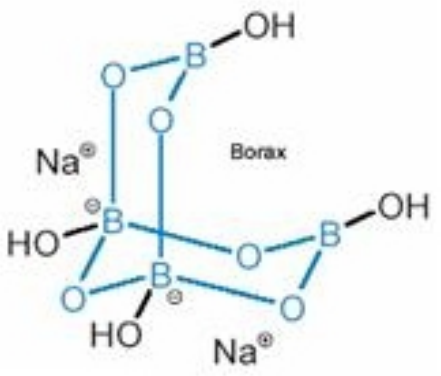

Figure 10. *Chemical structure of Borax, $Na_2B_2O_7{\cdot}4H_2O$.*

4.4. Data processing

NMR data were processed on an off-line computer using either the homemade program NMRLV or matNMR (11) (public domain NMR processing software running under MatLab (Mathworks, Natick, MA)). The FID data were read into the memory, zero-filled to 8196 points, Fourier-transformed, and phase-corrected.

Chapter 5. RESULTS AND DISCUSSIONS

5.1. Lineshape Simulation

The simulated spectra in Fig. 11 indicate that the width of the NMR line of the simulated spectrum is proportional to the coupling constant C_Q, as expected. The powder double peaks collapse into a single broad peak at low coupling constant, say C_Q = 0.5 and 1.0 MHz.

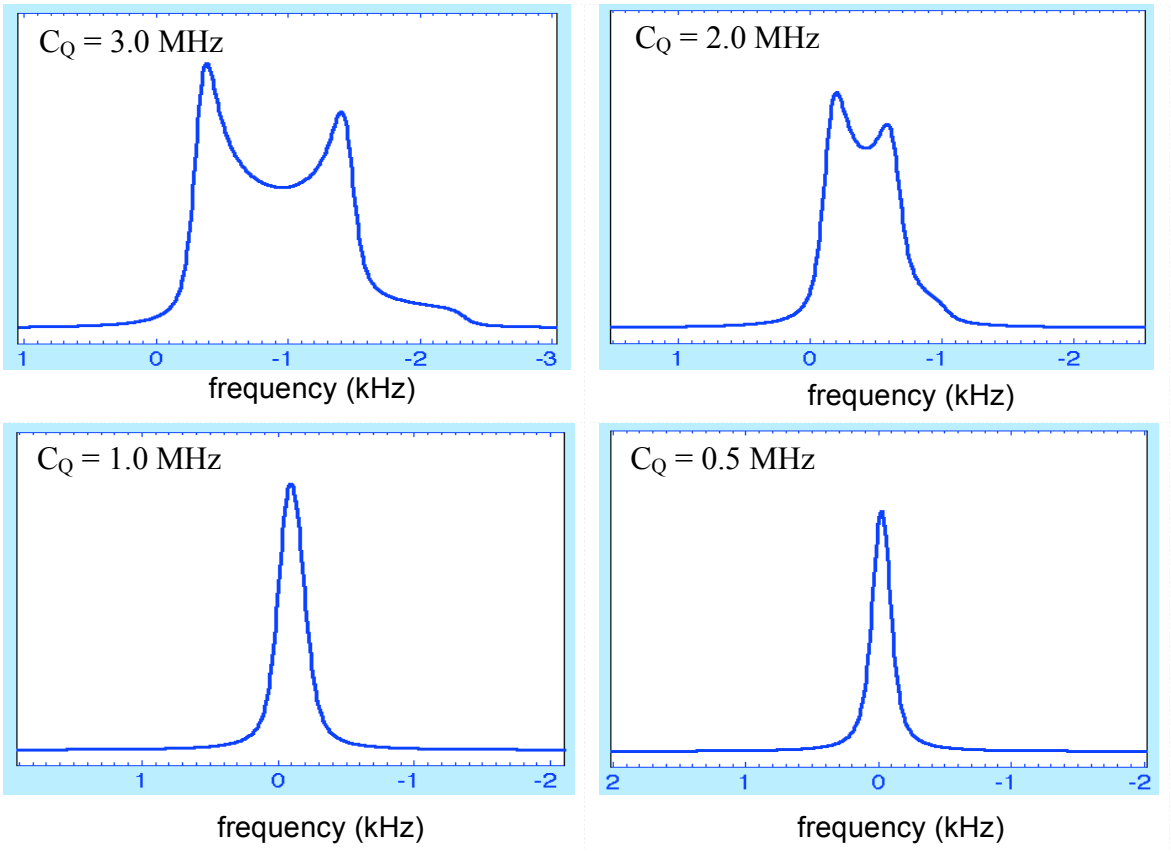

Figure 11. *Simulated powder spectra using Express for 6-site planar jumping motion with jump rate of 5 GHz, 10 kHz MAS spinning rate, and various quadrupolar coupling constants C_Q = 0.5, 1.0, 2.0, and 3.0 MHz. Line broadening of 100 Hz Gaussian and 100 Hz Lorentzian was applied.*

5.2. ^{11}B NMR measurement of Background

The NMR spectra in Fig. 12 represent three experiments conducted with PSW. Fig. 12a and 12b are the spectra obtained without MAS, and Fig. 12c is with 20 kHz MASR. ZGBS is expected to suppress the signal outside the coil. The broad signal in Fig. 12a is completely suppressed in Fig. 12b. If the broad peak in 11a were from the rotor, PSW, or the sample tube, sharp peaks would be visible in 12c. These confirm that the broad boron signal is from the boron nitride of the probe body. Because PSW does not contain any boron, these experiments simulate the experiment without a rotor.

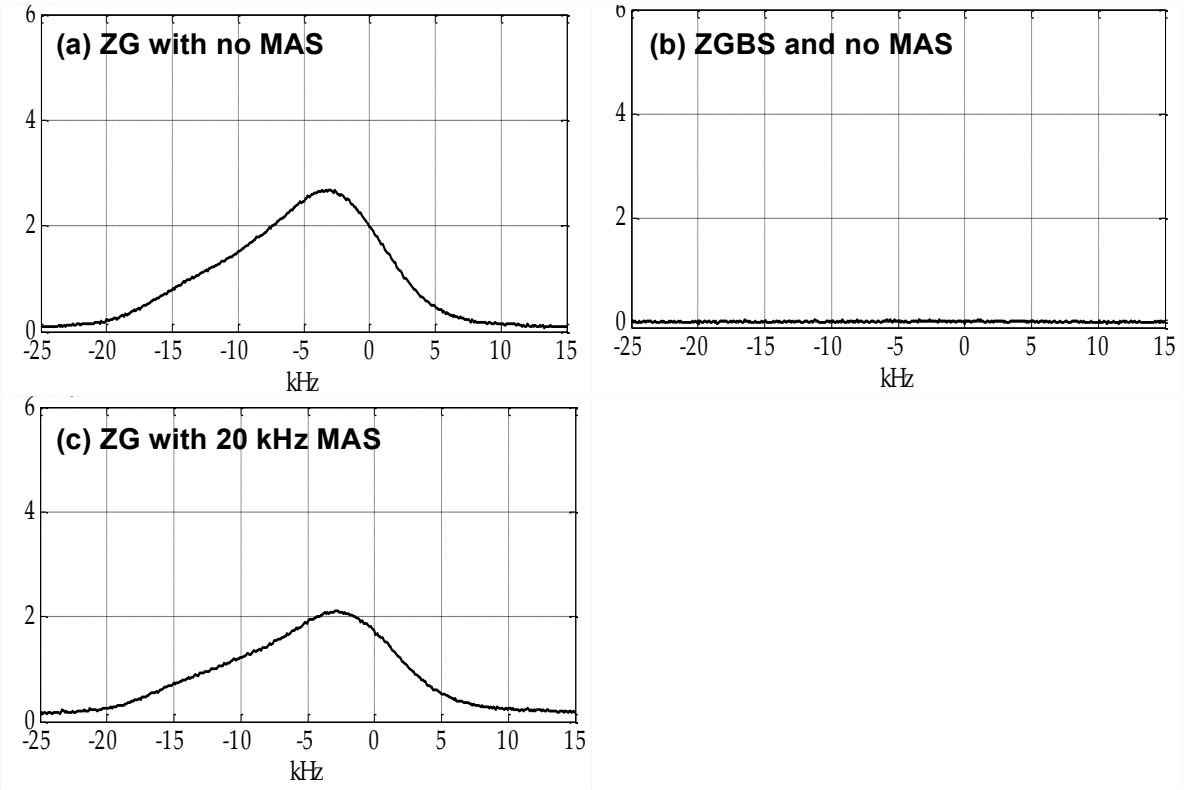

Figure 12. *^{11}B NMR signal from the probe, (a, c) without and (b) with background suppression, and (a, b) without and (c) with MAS. These observations, showing that the signal is completely suppressed by ZGBS in (b) and the sharp MAS peak is not visible in (c), indicate that this broad peak is from outside the rotor.*

5.3. ^{11}B NMR of Borax

Figs. 13 and 14 show ^{11}B NMR spectra without and with background suppression for a borax sample in a 2.5 mm rotor with MAS (30 kHz spinning rate, recycling time of 4 sec and 2.5 μs of 90° RF pulse width at set-point temperature 330 K). The broad signal in Fig. 13 originates from the probe background, as shown in Fig. 12. This probe background signal is clearly suppressed by ZGBS, as indicated in Fig. 14.

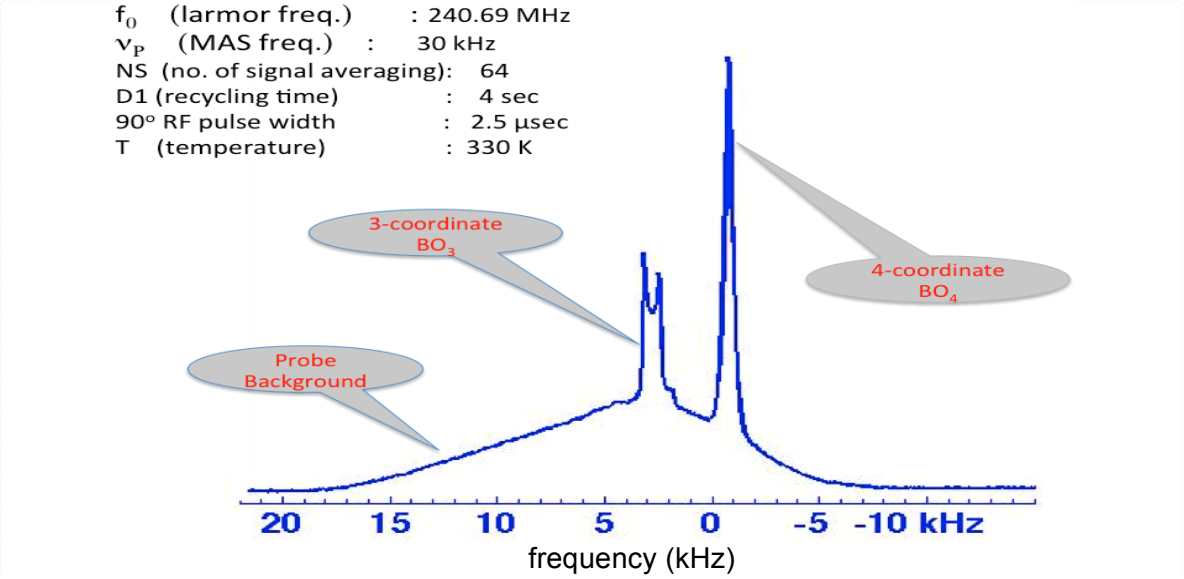

Figure 13. *^{11}B NMR spectrum of $Na_2B_2O_7{\cdot}4H_2O$. Broad line is the NMR signal from the background sample probe, which is known to contain ^{11}B nuclei. It is evident that the C_Q of the background ^{11}B NMR is huge, compared with that of borax. (Processed using NMRLV)*

The ^{11}B NMR spectrum in Fig. 14 is expected to have two major ^{11}B NMR peaks from 3-coordinate and 4-coordinate boron sites. Because the quadrupolar interaction is far more significant than the dipolar interaction for ^{11}B NMR, the line shape of the doublet peak for the 3-coordinate BO_3 is characteristic of a second order quadrupolar

contribution. It is also important to note the asymmetry in the 3-coordinate and 4-coordinate sites. This is due to the difference in the magnitudes of the electric field gradient that two nuclei experience, as demonstrated in the simulation plots in Fig. 11. With low C_Q, the quadrupolar effect will be weak and thus the splitting will not be as evident as it in the case of high C_Q. Thus, the 3-coordinate boron nuclei have a larger C_Q, while the 4-coordinate boron nucleus doesn't exhibit a doublet line shape due to its small quadrupolar coupling constant.

Peak intensity is another important consequence of site symmetry. The area under 3-coordinate and 4-coordinate peaks must be identical because the structure implies the same number of nuclei in each peak. In the case of the 4-coordinate boron nucleus's peak, where the peak doublet is not visible, the intensity is concentrated over a narrow range of frequencies and thus the peak is taller. On the other hand, the 3-coordinate boron signal shows a broader range of frequencies.

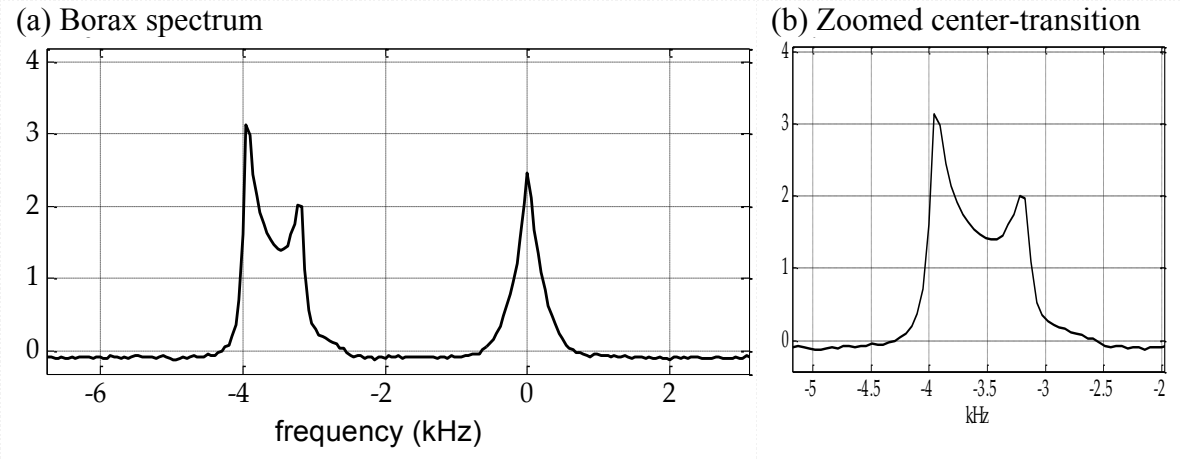

Figure 14. *(a) ^{11}B NMR spectrum of $Na_2B_2O_7{\cdot}4H_2O$ with ZGBS, and (b) zoomed doublet. Background broad peak, which is present in Fig. 13, is completely suppressed using composite 90^o RF pulses. The full-width-half-maximum (FWHM) of the doublet is 1.0 kHz.*

5.4. ^{11}B NMR of Diazaborine

The measured NMR spectrum of the diazaborine sample is shown in Fig. 15a. To determine whether the spectrum in Fig. 15a is from the diazaborine itself or a degradation product, a simulation experiment was performed using 2 site jumping with a jumping rate of 10 Hz, $C_Q = 1.25$ MHz, $\eta = 0.256$, 50 kHz spectral width, and MAS spinning rate 10 kHz. The simulated (or expected) width of the spectrum is about 0.2 kHz for the doublet of the central transition, as indicated in Fig. 15b. However, the width of the central transition in the measured spectrum is about 5 kHz, which is 25 times that of the simulated spectrum. This increased spectral linewidth is much closer to that of boron in borax, which is shown in Fig. 14b.

This result indicates that the diazaborine sample was probably completely degraded and oxidized before it reached the spectrometer, despite extra care. Note that the spectrum in Fig. 15a was obtained with 2048 scans and a relaxation delay of 30 seconds. These conditions were needed to obtain a usable signal, which was found, as expected, to be much weaker than the borax signal. The background suppression sequence has the incidental effect of partially suppressing signal from the satellite transitions of boron inside the sample coil. There is no hint of a line resembling the simulated powder pattern for diazaborine. Moreover, the long relaxation delay needed to acquire the spectrum indicates the absence of fast, large angle jumps. In fact, the narrow lines we observe in Fig. 15a are strongly reminiscent of 4-coordinate boron in borax, and it is very likely that a combination of atmospheric oxygen and water vapor produced degradation products with tetrahedral BO_4 coordination. The Fig. 15a shows slight left shift of the overall

spectral line, which would be due to the chemical shift. This trait is shared with the 3-coordinate boron-site peak of borax's ^{11}B NMR spectrum in Fig. 13.

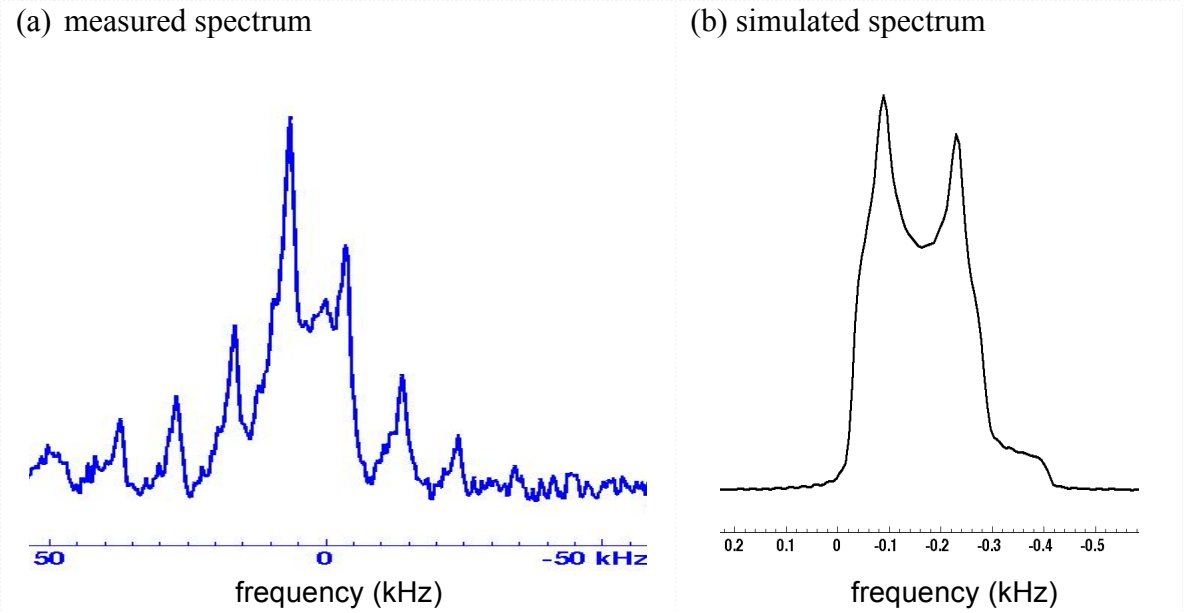

Figure 15. (a) *^{11}B NMR spectrum of diazaborine sample and (b) simulated spectrum. The width of the largest peak is about 5 kHz in the measured spectrum, while that of the simulated spectrum is about 0.2 kHz.*

Chapter 6. CONCLUSIONS

This thesis attempts to examine the molecular dynamics of 1,2-Dihydroazaborine-chromium tricarbonly using ^{11}B NMR experiments and line shape simulation of the central transition of ^{11}B for the planar jumping motion.

The measured ^{11}B NMR spectrum revealed two characteristic properties: (1) an order of magnitude greater line width than the simulated spectrum for the central transition using the reported C_Q and asymmetry, and (2) a long T_1 relaxation time. The broad spectrum rather mimics ^{11}B NMR of borax. The estimated T_1 is far too long for the fast-paced site jumping planar motion of the diazaborine, which should have had a very short T_1. These may indicate that the measured spectrum represents the signals of a 3-coordinate boron-oxygen-based compound that is a product of diazaborine degradation due to the diazaborine's likely contact with the air and moisture of the atmosphere. With the lack of enough sample and time, further study with varying sample temperatures was halted.

For further experiments, one must be very cautious about the extreme air and moisture sensitivity of the 1,2-Dihydroazaobinr-chromium tricarbonyl. Some suggestions include use of an O-ring for better sealing of the sample space at the NMR rotor ends, use of a glove box for sample preparation, and quicker experimentation procedures.

REFERENCES

1. Daly AM, Tanjaroon C, Marwitz AJ, Liu SY, Kukolich SG. Microwave spectrum, structural parameters, and quadrupole coupling for 1,2-dihydro-1,2-azaborine. J Am Chem Soc 2010;132(15):5501-5506.
2. Marwitz AJ, Matus MH, Zakharov LN, Dixon DA, Liu SY. A hybrid organic/inorganic benzene. Angew Chem Int Ed Engl 2009;48(5):973-977.
3. Duer MJ. Introduction to Solid-State NMR Spectroscopy: Wiley-Blackwell; 2005.
4. Vold RL, Hoatson GL. Effects of jump dynamics on solid state nuclear magnetic resonance line shapes and spin relaxation times. J Magn Reson 2009;198(1):57-72.
5. Farrar TC, Becker ED. Pulse and Fourier Transform NMR: Introduction to Theory and Methods. New York: Academic Press; 1971.
6. Slichter CP. Principles of Magnetic Resonance. Berlin, Germany: Springer-Verlag; 1990.
7. Griffiths DJ. Introduction to Quantum Mechanics. Upper Saddle River, NJ: Prentice Hall, Inc.; 1994.
8. Ashbrook S. Lecture note: Introduction to Quadruploar NMR, http://web.mac.com/jeremytitman/Solid-state_NMR_Group/Stellenbosch_Workshop_files/IntroToQuadrupolarNMR.pdf.
9. Griffiths DJ. Introduction to Electrodynamics. Upper Saddle River, NJ: Prentice Hall, Inc.; 1999.
10. Cory DG, Ritchey WM. Suppression of signals from the probe in bloch decay spectra. Jour Magn Reson 1988;80(1):128-132.

11. van Beek JD. matNMR: a flexible toolbox for processing, analyzing and visualizing magnetic resonance data in Matlab. J Magn Reson 2007;187(1):19-26.